Available online at www.sciencedirect.com
SCIENCE DIRECT®
ELSEVIER
International Journal of Solids and Structures 42 (2005) 4030–4057
INTERNATIONAL JOURNAL OF SOLIDS and STRUCTURES
www.elsevier.com/locate/ijsolstr

Meshfree analysis of softening elastoplastic solids using variational multiscale method

Jeoung-Heum Yeon, Sung-Kie Youn *

Department of Mechanical Engineering, Korea Advanced Institute of Science and Technology, 373-1, Gusung-dong, Yusung-ku, Taejon 305-701, Korea

Received 29 November 2004
Available online 26 January 2005

Abstract

A meshfree multiscale method is presented for efficient analysis of elastoplastic solids. In the analysis of softening elastoplastic solids, standard finite element methods or meshfree methods typically yield mesh-dependent results. The reason for this well-known effect is the loss of ellipticity of the boundary value problem. In this work, the scale decomposition is carried out based on a variational form of the problem. A coarse scale is designed to represent global behavior and a fine scale to represent local behavior. A fine scale region is detected from the local failure analysis of an acoustic tensor to indicate a region where deformation changes abruptly. Each scale variable is approximated using a meshfree method. Meshfree approximation is well-suited for adaptivity. As a method of increasing the resolution, a partition of unity based extrinsic enrichment is used. In particular, fine scale approximations are designed to appropriately represent local behavior by using a localization angle. Moreover, the regularization effect through the convexification of non-convex potential is embedded to represent fine scale behavior. Each scale problem is solved iteratively. The proposed method is applied to shear band problems. In the results of analysis about pure shear and compression problems, straight shear bands can be captured and mesh-insensitive results are obtained. Curved shear bands can also be captured without mesh dependency in the analysis of indentation problem.

Keywords: Variational multiscale; Meshfree; Meshless; Elastoplasticity; Shear band

* Corresponding author. Tel.: +82 428693074; fax: +82 428693095.
E-mail addresses: jhyeon@kaist.ac.kr (J.-H. Yeon), skyoun@sorak.kaist.ac.kr (S.-K. Youn).

0020-7683/$ - see front matter © 2004 Elsevier Ltd. All rights reserved.
doi:10.1016/j.ijsolstr.2004.12.007

1. Introduction

In the deformation analysis of strain-softening elastoplastic solids, the localization phenomenon arises. Strain concentration occurs within a critical zone as a consequence of the bifurcation of the local constitutive behavior of the material. Such critical zones, for example, shear bands, are observed in metals as well as in geomaterials. Applications of standard finite element methods or meshfree methods to the simulation of shear bands in strain-softening elastoplastic solids typically yield mesh-dependent post-critical results. It is due to the loss of ellipticity of boundary value problem. This leads to ill posedness of the problem and lack of objectivity.

To obtain objective results without mesh dependency, a plethora of research has been conducted including regularization effects. Among topics of these studies are viscoplastic regularization, nonlocal regularization, gradient regularization and coupled stress regularization. Needleman (1988) proposed regularization by introducing rate-dependency in the material. Bazant (1984) and Bazant and Lin (1988) used non-local regularization by introducing the constitutive equations with a function of nonlocal variables. Gradient type regularization with the gradient-dependent softening plasticity theory was developed by Zbib and Aifantis (1988), Muhlhaus and Aifantis (1991) and others. de Borst and Sluys (1991) used micro-polar Cosserat theories to introduce regularization effects. Miehe and Lambrecht (2003) proposed a regularization method through the convexification of non-convex potential.

In another point of view, the strain localization phenomena involve a narrow region with a high displacement gradient along the width of the band. A natural approximation method of displacement is suggested by a smooth function representing the coarse scale behavior in the entire region added by a sharp function representing the fine scale behavior in the localization region. This approach is one of the multiscale methods that analyzes a problem with different scales. In general, to accurately solve problems of this sort, the domain must be discretized into very fine meshes to capture the local behavior, however, this process is inefficient and very costly. For the efficient analysis of these problems, many attempts have been undertaken. Many kinds of adaptive schemes are suggested by Zienkiewicz and Taylor (1989). In most of the adaptive schemes, error estimation is required to detect large error regions. The decomposition of these problems into coarse scales and fine scales is an efficient way to solve the problems. Direct decomposition of the variational form of the governing equations is called the variational multiscale method, which was proposed by Hughes (1995) and Hughes et al. (1998) and was applied to the Helmholtz equation (Oberai and Pinsky, 1998), strain localization problem (Garikipati and Hughes, 1998, 2000), and eddy flow problem (Hughes et al., 2001a,b). Zohdi et al. (1996) and Oden and Zohdi (1997) proposed a multiscale method based on the homogenization scheme to analyze behavior of the heterogeneous material. They made a coarse scale model using homogenization to determine the overall behavior and a fine scale model, using a detailed model, to determine local behavior. They applied these methods to the analysis of heterogeneous material and composite material (Oden et al., 1999). Liu and Chen (1995) and Liu et al. (1996) used the low-pass filter property of meshfree shape function, and they detected large error region by using that property and applied adaptive scheme. In the meshfree method, adaptivity is easy to implement because no elements are employed. Li and Liu (1999a,b) generalized moving least-squares approximation and made a hierarchical partition of unity. They applied this scheme to multiscale problems such as shear band analysis.

In this paper, a variational multiscale method is adopted to solve the elastoplastic deformation problem. From the local failure analysis of the acoustic tensor, bifurcation regions are detected and used as fine scale regions. Bifurcation direction is used to approximate fine scale to appropriately represent local behavior. Each scale problem is solved iteratively, and, consequently, converged results are obtained. Iteration procedure is indispensable for the elastoplastic deformation analysis, so, this kind of solution procedure is adequate for the elastoplastic deformation problem. As an approximation method, the moving least-squares meshfree method is adopted. In this scheme, adaptivity can be efficiently applied. Coarse scale variables

are approximated with the original moving least-squares shape functions, and fine scale variables are approximated with the enriched shape function associated with partition of unity method. As numerical examples, pure shear, compression and indentation problems are solved. These examples represent straight and curved shear bands, respectively.

This paper is organized as follows. In the next section, various numerical formulations of elastoplastic deformation problems are described. A regularization method which utilizes convexification is described in Section 3, and multiscale formulation and numerical implementations are described in Section 4. Numerical examples which show the validity of the proposed method are given in Section 5. A summary and some concluding remarks are provided in the last section.

2. Formulation of the elastoplastic deformation problem

2.1. Weak form of the elastoplastic problem

The deformation of elastoplastic solids is governed by the equations of motion, boundary conditions and constitutive relations. The governing equations are in non-linear form, so, we use the Newton method to linearize these equations.

Let the index of the loading step be 'n', and the index of Newton iteration step be 'i'. The i-th iteration step during n-th loading step can be written as (n,i). The governing equations can be written as follows:

$$\frac{\partial \sigma_{ij}^{(n,i+1)}}{\partial x_i} + \rho b_j^{(n+1)} = 0 \text{ in } V, \tag{1}$$

where σ_{ij} denotes the Cauchy stress tensor, ρ the mass density, b_j the body force. Superscripts indicate configuration of variables. Displacement and traction boundary conditions can be written as follows:

$$u_i^{(n+1)} = g_i^{(n+1)} \text{ on } S_u, \tag{2}$$

$$\sigma_{ij}^{(n+1)} n_i = t_j^{(n+1)} \text{ on } S_t, \tag{3}$$

where g_i and t_i are given displacement and traction.

The stress at $(n,i+1)$ step can be represented as follows:

$$\sigma_{ij}^{(n,i+1)} = \sigma_{ij}^{(n,i)} + \Delta\sigma_{ij}^{(n,i+1)}. \tag{4}$$

The weak form of the governing equations can be written as follows:

$$\int_V \frac{\partial w_j}{\partial x_i} \Delta\sigma_{ij}^{(n,i+1)} \,\mathrm{d}V = \int_{S_t} w_j t_j^{(n+1)} \,\mathrm{d}S - \int_V \frac{\partial w_j}{\partial x_i} \sigma_{ij}^{(n,i)} \,\mathrm{d}V + \int_V w_j \rho b_j^{(n+1)} \,\mathrm{d}V, \tag{5}$$

where w_j is the test function that has zero value on S_u.

As a plasticity model, a von Mises-type model (J_2 flow rule) is used in this work. A yield function of J_2 flow rule is written as follows:

$$\Phi(\sigma, \bar{\varepsilon}^{\mathrm{p}}) = \sqrt{\frac{3}{2}\sigma'_{ij}\sigma'_{ij}} - \sigma_{\mathrm{Y}}(\bar{\varepsilon}^{\mathrm{p}}), \tag{6}$$

where σ'_{ij} denotes deviatoric stress and σ_{Y} the yield stress. $\bar{\varepsilon}^{\mathrm{p}}$ indicates effective plastic strain, and its time rate is defined as $\dot{\bar{\varepsilon}}^{\mathrm{p}} = \sqrt{2/3\dot{\varepsilon}_{ij}^{\mathrm{p}}\dot{\varepsilon}_{ij}^{\mathrm{p}}}$.

Strain can be decomposed into elastic and plastic parts.

$$\dot{\varepsilon}_{ij} = \dot{\varepsilon}_{ij}^{\mathrm{e}} + \dot{\varepsilon}_{ij}^{\mathrm{p}}. \tag{7}$$

Elastic strain and stress has the following relations:

$$\dot{\sigma}_{ij} = E_{ijkl}\dot{\varepsilon}^{\mathrm{e}}_{ij} = (E^{\mathrm{s}}_{ijkl} + E^{\mathrm{d}}_{ijkl})\dot{\varepsilon}^{\mathrm{e}}_{ij}, \tag{8}$$

where E_{ijkl} denotes elastic modulus tensor. Spherical and deviatoric parts are written as

$$E^{\mathrm{s}}_{ijkl} = \kappa\delta_{ij}\delta_{kl}, \tag{9}$$

$$E^{\mathrm{d}}_{ijkl} = 2\mu[(\delta_{ik}\delta_{jl} + \delta_{il}\delta_{jk})/2 - (\delta_{ij}\delta_{kl})/3], \tag{10}$$

$\kappa$and μ indicates the bulk modulus and shear modulus respectively.

From the associative flow rule, plastic strain can be written as

$$\dot{\varepsilon}^{\mathrm{p}}_{ij} = \dot{\lambda}\frac{\partial \Phi}{\partial \sigma_{ij}}, \tag{11}$$

where λ denotes plastic multiplier.

The linear hardening/softening rule is represented as follows:

$$\sigma_Y = Y_0 + h\bar{\varepsilon}^{\mathrm{p}}, \tag{12}$$

where Y_0 denotes initial yield stress, h the coefficient of linear hardening/softening.

From the above elastoplastic constitutive relations, the increment of stress can be represented as follows:

$$\Delta\sigma^{(n,i+1)}_{ij} = C_{ijkl}\Delta\varepsilon^{(n,i+1)}_{ij}. \tag{13}$$

The explicit tensor form of C_{ijkl} can be written as

$$C = E^{\mathrm{s}} + \left[1 - \frac{1}{1+h/3\mu}\frac{\Phi^{\mathrm{trial}}_{n+1}}{\|\mathrm{dev}(\sigma^{\mathrm{trial}}_{n+1})\|}\right]E^{\mathrm{d}} - \frac{2\mu}{1+h/3\mu}\left[1 - \frac{\Phi^{\mathrm{trial}}_{n+1}}{\|\mathrm{dev}(\sigma^{\mathrm{trial}}_{n+1})\|}\right]N^{\mathrm{trial}}_{n+1}\otimes N^{\mathrm{trial}}_{n+1}, \tag{14}$$

where superscript 'trial' indicates the elastic-trial state and $N^{\mathrm{trial}}_{n+1} = \mathrm{dev}(\sigma^{\mathrm{trial}}_{n+1})/\|\mathrm{dev}(\sigma^{\mathrm{trial}}_{n+1})\|$. Detailed derivations can be found in referring article (Simo and Hughes, 1998).

Finally, the weak form of the governing equations (5) can be rewritten as

$$\int_V \frac{\partial w_j}{\partial x_i} C_{ijkl}\Delta\varepsilon^{(n,i+1)}_{kl}\,\mathrm{d}V = -\int_V \frac{\partial w_j}{\partial x_i}\sigma^{(n,i)}_{ij}\,\mathrm{d}V + \int_{S_t} w_j t^{(n+1)}_j\,\mathrm{d}S + \int_V w_j\rho b^{(n+1)}_j\,\mathrm{d}V. \tag{15}$$

The trial function space and test function space are defined as follows:

$$U = \{v \mid v \in H^1(V), v = \Delta g^{(n+1)} \text{ at } S_u\}, \quad \Delta u^{(n,i+1)} \in U, \tag{16}$$

$$V = \{w \mid w \in H^1(V), w = 0 \text{ at } S_u\}, \quad w \in V. \tag{17}$$

2.2. Incremental variational formulation of the elastoplastic problem

The elastoplastic problem stated in the above section can also be described in incremental variational form. To do this, the concept of an incremental stress potential W is required. W is defined on the time interval $[t_n, t_{n+1}]$ and has the following property.

$$\sigma^{(n,i+1)} = \partial_\varepsilon W(\varepsilon^{(n,i+1)}). \tag{18}$$

To satisfy the above equation, W has the following form for the standard dissipative material.

$$W(\varepsilon^{(n,i+1)}) = \inf_{\varphi}\int_{t_n}^{t_{n+1}}[\dot{\psi} + \phi]\mathrm{d}t = \inf_{\varphi}\int_{t_n}^{t_{n+1}}[\sigma : \dot{\varepsilon}]\mathrm{d}t. \tag{19}$$

Here, φ indicates internal variables, $\psi = \psi(\varepsilon, \varphi)$ energy storage function, $\phi = \phi(\dot{\varphi})$ dissipation function. More detailed properties about standard dissipative material can be found in the referring article (Miehe, 2000).

The elastoplastic problem can be represented as the variational form of incremental potential energy defined below.

$$\Pi(u^{(n,i+1)}) = \int_V [W(\varepsilon^{(n,i+1)}) - u^{(n,i+1)} \cdot b^{(n+1)}] \mathrm{d}V - \int_{S_t} u^{(n,i+1)} \cdot t^{(n+1)} \mathrm{d}S. \tag{20}$$

Displacement at $(n, i+1)$ is written as $u^{(n,i+1)} = u^{(n,i)} + \Delta u^{(n,i+1)}$, and its variation is written as

$$\delta u^{(n,i+1)} = \delta \Delta u^{(n,i+1)}. \tag{21}$$

Taking the variation of Eq. (20) leads to

$$\delta \Pi(u^{(n,i+1)}) = \int_V [\delta W(\varepsilon^{(n,i+1)}) - \delta \Delta u^{(n,i+1)} \cdot b^{(n+1)}] \mathrm{d}V - \int_{S_t} \delta \Delta u^{(n,i+1)} \cdot t^{(n+1)} \mathrm{d}S = 0. \tag{22}$$

The variation of incremental stress potential can be summarized as follows:

$$\begin{aligned} \delta W(\varepsilon^{(n,i+1)}) &= \partial_{\varepsilon} W(\varepsilon^{(n,i+1)}) : \delta \varepsilon^{(n,i+1)} = \sigma^{(n,i+1)} : \delta \Delta \varepsilon^{(n,i+1)} = (\sigma^{(n,i)} + \Delta \sigma^{(n,i+1)}) : \delta \Delta \varepsilon^{(n,i+1)} \\ &= (\sigma^{(n,i)} + C : \Delta \varepsilon^{(n,i+1)}) : \delta \Delta \varepsilon^{(n,i+1)}. \end{aligned} \tag{23}$$

Inserting this relation to Eq. (22) leads to the same form as Eq. (15).

2.3. Local failure analysis

In this section, some aspects of the general theory of localization of inelastic deformations are revisited. Some of the basic principles underlying the theory follow the Hadamard's studies on stability (Hadamard, 1903). In the deformation process of strain softening material, a bifurcation can occur in such a manner that subsequent deformations become discontinuous across a plane of orientation n.

Let u be the displacement field in the solid. Displacement gradient exhibits a jump across the plane of discontinuity. Maxwell's compatibility condition indicates the jump is of the form

$$\lfloor\!| \Delta u_{i,j} |\!\rfloor = g_i n_j = g m_i n_j \tag{24}$$

for the vector g, where m is the unit vector along g.

Therefore, the corresponding strain jump can be written as

$$[\!| \Delta \varepsilon_{ij} |\!] = \frac{1}{2} g (m_i n_j + m_j n_i). \tag{25}$$

Stress–strain relations take the form as in Eq. (13). Taking the jumps leads to

$$\lfloor\!| \Delta \sigma_{ij} |\!\rfloor = C_{ijkl} [\!| \Delta \varepsilon_{kl} |\!]. \tag{26}$$

From the traction continuity across the discontinuity plane, the following equations must be satisfied.

$$\lfloor\!| \Delta t_j |\!\rfloor = \lfloor\!| n_i \Delta \sigma_{ij} |\!\rfloor = n_i \lfloor\!| \Delta \sigma_{ij} |\!\rfloor = 0. \tag{27}$$

Using the kinematic relation (25) and with the above equations, it follows that

$$(n_i C_{ijkl} n_l) m_k = A_{jk}(n) m_k = 0. \tag{28}$$

This condition indicates that acoustic tensor $A(n)$ must have zero eigenvalue for the localized mode to be possible. It means that the direction n that satisfies

$$\det[A(n)] = 0 \tag{29}$$

is the localization direction.

In the two-dimensional case, n can be written as

$$n = c\mathbf{e_1} + s\mathbf{e_2} \text{ with } c = \cos\theta \text{ and } s = \sin\theta. \tag{30}$$

Eq. (29) can be written as

$$\det[A(n)] = a_1c^4 + a_2c^3s + a_3c^2s^2 + a_4cs^3 + a_5s^4 = 0. \tag{31}$$

The coefficients a_i are appeared to contain simple arithmetic of components C_{ijkl}. Detailed equations can be found in the referring article (Ortiz et al., 1987).

Dividing Eq. (31) by positive number $\cos^4\theta$, it follows that

$$f(x) = a_5x^4 + a_4x^3 + a_3x^2 + a_2x + a_1 = 0. \tag{32}$$

The polynomial $f(x)$ is positive everywhere prior to localization and has zero value at the onset of localization. Therefore, the localization can be possible at the minima of $f(x)$. These occur at the roots of the cubic polynomial $f'(x)$, which can be computed in the closed form by means of Cardan's formulae.

3. Convexification of incremental stress potential

3.1. Convexity conditions

Applications of standard finite element methods or meshfree methods to the simulation of shear bands in strain-softening elastoplastic solids yield mesh-dependent results. The reason is known to be the loss of ellipticity of the boundary value problem.

Consequently, an enormous amount of research has been conducted including regularization effects. Representatives of the research are viscoplastic regularization, nonlocal regularization, gradient regularization, and coupled stress regularization: see, for example, Needleman (1988), Bazant and Lin (1988), Muhlhaus and Aifantis (1991) and Muhlhaus and Vardoulaks (1987). Miehe and Lambrecht (2003) proposed a regularization method through the convexification of non-convex potential. The convexity of incremental stress potential is strongly related with material stability.

Firstly, we can consider quasi-convexity of incremental stress potential W which is said to be quasi-convex at ε if the condition

$$\frac{1}{|D|}\int_V W(\varepsilon + \mathrm{sym}[\nabla w])\mathrm{d}V \geqslant W(\varepsilon) \tag{33}$$

holds for ∇w such that $w = 0$ on ∂D. Here, D is an arbitrarily chosen part of the domain. This condition states that for all fluctuations w on D, ε provides an absolute minimizer of the incremental stress potential in D. This weak convexity condition was introduced by Morrey (1952). Quasi-convexity ensures the first term in the right hand side of incremental potential energy in Eq. (20) $\int_V W(\varepsilon)\mathrm{d}V$ to be sequentially weakly lower semi-continuous. Quasi-convexity is the key property for the existence of sufficiently regular minimizer of the variational problem (22). Further details of the existence theorem can be found in references (Ball, 1977; Ciarlet, 1988).

The quasi-convexity condition based on an integral condition is hard to apply in practice. Therefore, we can consider the slightly weaker condition of rank-one convexity. W is said to be rank-one convex at ε if the condition

$$\xi W(\varepsilon^+) + (1-\xi)W(\varepsilon^-) \geqslant W(\varepsilon) \tag{34}$$

holds for the laminate strains ε^+ and ε^-, which satisfy the conditions

$$\varepsilon = \xi\varepsilon^+ + (1-\xi)\varepsilon^- \text{ and } \mathrm{rank}[\varepsilon^+ - \varepsilon^-] \leqslant 1 \tag{35}$$

in terms of the scalar $\xi \in [0,1]$. The difference of the two laminate strains can be written in the form $\mathrm{sym}[m \otimes n]$ because the rank of the difference is less than one. Here, m and n are any vectors. The Taylor series expansion of Eq. (34) provides the infinitesimal rank-one convexity condition

$$(m \otimes n) : \partial^2_{\varepsilon\varepsilon} W(\varepsilon) : (m \otimes n) \geqslant 0, \tag{36}$$

where $\partial^2_{\varepsilon\varepsilon} W(\varepsilon)$ is the tangent modulus identical to C used in Eq. (14). Applying the minor symmetry of tangent modulus, Eq. (36) can be written as

$$m \cdot (A(n) \cdot m) \geqslant 0, \tag{37}$$

where $A(n)$ is the acoustic tensor used in Eq. (28). This inequality indicates that $A(n)$ has to have positive eigenvalues for the rank-one convex incremental stress potential. In the failure case of this convexity condition, $A(n)$ has an eigenvalue of zero. This is the same condition as the local failure condition in Section 2.3.

3.2. Convexifications

The non-convex variational problem can be relaxed by using the convexified incremental stress potential. Convexification of W can be done by constructing its convex envelop W_R. A rank-one convex envelope is defined by the minimization problem

$$W_R(\varepsilon) = \inf_{\xi_i, \varepsilon_i} \left\{ \sum_{i=1}^{N} \xi_i W(\varepsilon_i) \right\} \tag{38}$$

with

$$\sum_{i=1}^{N} \xi_i = 1, \quad \varepsilon = \sum_{i=1}^{N} \xi_i \varepsilon_i, \text{ and } \operatorname{rank}\lfloor \varepsilon_i - \varepsilon_j \rfloor \leqslant 1 \quad i,j = 1,2,\ldots,N. \tag{39}$$

Here, N is the number of phases, and in the ideal case, N is infinity. To represent a more systematic form, the following approximate convexification is possible.

$$W_{R_0}(\varepsilon) = W(\varepsilon), \tag{40}$$

$$W_{R_k}(\varepsilon) = \inf_{\xi^{\pm}, \varepsilon^{\pm}} \{ \xi^{+} W_{R_{k-1}}(\varepsilon^{+}) + \xi^{-} W_{R_{k-1}}(\varepsilon^{-}) \} \quad k = 1,2,\ldots. \tag{41}$$

After an infinite number of steps, the exact rank-one convexified potential is obtained.

$$W_R(\varepsilon) = \lim_{k \to \infty} W_{R_k}(\varepsilon). \tag{42}$$

As an approximation of rank-one convexification, level-1 approximation can be used:

$$W_{R_1}(\varepsilon) = \inf_{\xi, \varepsilon^{\pm}} \{ \xi W(\varepsilon^{+}) + (1-\xi) W(\varepsilon^{-}) \} \tag{43}$$

with

$$\varepsilon = \xi \varepsilon^{+} + (1-\xi)\varepsilon^{-}. \tag{44}$$

The difference of two laminate strains can be written as a symmetric part of the tensor product of any two vectors.

$$\varepsilon^{+} - \varepsilon^{-} = d\,\mathrm{sym}[m \otimes n], \tag{45}$$

where m and n are vectors and d indicates magnitude.

By using Eqs. (44) and (45), the two laminate strains can be represented as

$$\varepsilon^{+} = \varepsilon + d(1-\xi)\mathrm{sym}[m \otimes n], \tag{46}$$

$$\varepsilon^{-} = \varepsilon - d\xi\,\mathrm{sym}[m \otimes n]. \tag{47}$$

For the best approximation of rank-one convexification using level-1, we should set m and n as the vectors in Eq. (24).

$$m = [\cos\theta_c \quad \sin\theta_c], \quad n = [-\sin\theta_c \quad \cos\theta_c]. \tag{48}$$

The angle θ_c is determined by the local failure analysis and scalar ξ is a given value. The variation of relaxed incremental stress potential is written as

$$\delta W_{R_1^a}(\varepsilon) = \delta\Delta\varepsilon : (\sigma + C : \Delta\varepsilon) + \delta\Delta d : (\xi(1-\xi)\mathrm{sym}[m \otimes n] : C : \mathrm{sym}[m \otimes n])\Delta d. \tag{49}$$

The first term is the same as the conventional term in Eq. (23), and the second term plays a relaxation role.

As a viewpoint of enrichment, strain increment can be written as

$$\Delta\varepsilon = \Delta\bar{\varepsilon} + \Delta\hat{\varepsilon}. \tag{50}$$

Here, $\Delta\bar{\varepsilon}$ indicates conventional term and $\Delta\hat{\varepsilon}$ enriched term. The following approximation can represent convexification effects.

$$\Delta\hat{\varepsilon} = \Delta\tilde{d}\,\mathrm{sym}[m \otimes n], \tag{51}$$

where $\Delta\tilde{d}$ indicates any scalar that represents the magnitude of the enriched term.

These convexification can be interpreted as micro-structure development, as in Fig. 1. Here, θ_c is the critical angle calculated through local failure analysis, Δd the intensity of the micro-shearing, and δ the given a priori length scale.

Conversely, we can obtain the convexification effect by embedding the displacement of micro-structure to the conventional displacement approximation. A fine scale displacement field can be approximated as the displacement of a micro-structure.

A displacement field is divided into three parts: (1), (2), and (3), as in Fig. 1. In each part, x and y components of displacement can be written as follows:

$$\Delta\hat{u}_1 = \begin{cases} \Delta d/2\cos\theta_c & \text{at (1)} \\ \Delta d/\delta(-\sin\theta_c\cos\theta_c x + \cos^2\theta_c y) & \text{at (2)} \\ -\Delta d/2\cos\theta_c & \text{at (3)}, \end{cases} \tag{52}$$

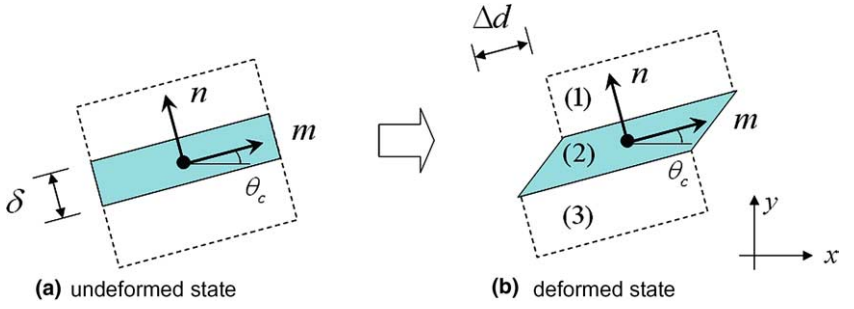

Fig. 1. Micro-structure development of convexification effect.

$$\Delta\hat{u}_2 = \begin{cases} \Delta d/2\sin\theta_c & \text{at (1)} \\ \Delta d/\delta(-\sin^2\theta_c x + \sin\theta_c\cos\theta_c y) & \text{at (2)} \\ -\Delta d/2\sin\theta_c & \text{at (3).} \end{cases} \tag{53}$$

By differentiating the displacement field in region (2), we can calculate the strain field.

$$\Delta\hat{\varepsilon}_{11} = \Delta d/\delta(-\sin\theta_c\cos\theta_c), \tag{54}$$

$$\Delta\hat{\varepsilon}_{22} = \Delta d/\delta(\sin\theta_c\cos\theta_c), \tag{55}$$

$$\Delta\hat{\varepsilon}_{12} = \Delta d/2\delta(\cos^2\theta_c - \sin^2\theta_c). \tag{56}$$

We can certify that the strain fields are compatible with relaxed strain as in Eq. (51). These displacement fields are to be embedded to approximate fine scale field in Section 4.2.

4. Variational multiscale formulation

4.1. Scale decomposition

The increment of displacement can be written as follows:

$$\Delta u = \Delta\bar{u} + \Delta\hat{u} = \Delta\bar{u} + \Gamma\Delta\hat{u}, \tag{57}$$

where $\Delta\bar{u}$ and $\Delta\hat{u}$ are the coarse and fine scale parts of displacement increment, respectively, and Γ is the fine scale switch that notifies nodes that fine scale enrichments are needed. In the fine scale region, Γ has a value of 1 and has zero value in the other region. We can define the trial function spaces of each scale as

$$\overline{U} = \{v \mid v \in H^1(V), v = \Delta g^{(n+1)} \text{ at } S_u\}, \quad \Delta\bar{u} \in \overline{U}, \tag{58}$$

$$\widehat{U} = \{v \mid v \in H^1(V), v = 0 \text{ at } S_u\}, \quad \Delta\hat{u} \in \widehat{U}, \tag{59}$$

$$U = \overline{U} \oplus \widehat{U}. \tag{60}$$

Test function can also be written in the decomposed form as follows:

$$w = \bar{w} + \Gamma\hat{w}, \tag{61}$$

where $\bar{w}$ and $\hat{w}$ are the coarse and fine scale parts, respectively. We can define test function spaces of each scale as follows:

$$\overline{V} = \{w \mid w \in H^1(V), w = 0 \text{ at } S_u\}, \quad \bar{w} \in \overline{V}, \tag{62}$$

$$\widehat{V} = \{w \mid w \in H^1(V), w = 0 \text{ at } S_u\}, \quad \hat{w} \in \widehat{V}, \tag{63}$$

$$V = \overline{V} \oplus \widehat{V}. \tag{64}$$

Since the test function is arbitrary for each function spaces, a weak form (15) can be decomposed into coarse scale part and fine scale part as follows:

$$\int_V \frac{\partial\bar{w}_j}{\partial x_i} C_{ijkl}(\Delta\bar{\varepsilon}_{kl} + \Gamma\Delta\hat{\varepsilon}_{kl})\,\mathrm{d}V = -\int_V \frac{\partial\bar{w}_j}{\partial x_i}\sigma_{ij}^{(n,i)}\,\mathrm{d}V + \int_S \bar{w}_j t_j^{(n+1)}\,\mathrm{d}S + \int_V \bar{w}_j \rho b_j^{(n+1)}\,\mathrm{d}V, \tag{65}$$

$$\Gamma\int_V \frac{\partial\hat{w}_j}{\partial x_i} C_{ijkl}(\Delta\bar{\varepsilon}_{kl} + \Gamma\Delta\hat{\varepsilon}_{kl})\,\mathrm{d}V = -\Gamma\int_V \frac{\partial\hat{w}_j}{\partial x_i}\sigma_{ij}^{(n,i)}\,\mathrm{d}V + \Gamma\int_S \hat{w}_j t_j^{(n+1)}\,\mathrm{d}S + \Gamma\int_V \hat{w}_j \rho b_j^{(n+1)}\,\mathrm{d}V. \tag{66}$$

Superscripts on the strain components are omitted for the convenience. The coarse scale problem (65) and the fine scale problem (66) can be arranged as follows:

$$\int_V \frac{\partial \bar{w}_j}{\partial x_i} C_{ijkl} \Delta\bar{\varepsilon}_{kl}\,\mathrm{d}V = -\int_V \frac{\partial \bar{w}_j}{\partial x_i}\sigma_{ij}^{(n,i)}\,\mathrm{d}V + \int_S \bar{w}_j t_j^{(n+1)}\,\mathrm{d}S + \int_V \bar{w}_j \rho b_j^{(n+1)}\,\mathrm{d}V - \Gamma\int_V \frac{\partial \bar{w}_j}{\partial x_i} C_{ijkl}\Delta\hat{\varepsilon}_{kl}\,\mathrm{d}V, \tag{67}$$

$$\Gamma\int_V \frac{\partial \hat{w}_j}{\partial x_i} C_{ijkl} \Delta\hat{\varepsilon}_{kl}\,\mathrm{d}V = -\Gamma\int_V \frac{\partial \hat{w}_j}{\partial x_i}\sigma_{ij}^{(n,i)}\,\mathrm{d}V + \Gamma\int_S \hat{w}_j t_j^{(n+1)}\mathrm{d}S + \Gamma\int_V \hat{w}_j \rho b_j^{(n+1)}\,\mathrm{d}V - \Gamma\int_V \frac{\partial \hat{w}_j}{\partial x_i} C_{ijkl}\Delta\bar{\varepsilon}_{kl}\,\mathrm{d}V. \tag{68}$$

In the coarse scale problem (67), we can see that the coarse scale variable appears only on the left-hand side, and fine scale variable only in the right-hand side. For the fine scale problem (68), fine scale variable appears only on the left-hand side. Notice that the fine scale problem is defined only in the fine scale region.

In the variational multiscale method proposed by Hughes (1995), the fine scale problem is solved first by an analytic approach, and the results are used to construct the coarse scale problem. By solving the coarse scale problem numerically, multiscale results are obtained. The solution procedure is appropriate for the problem whose analytic solution of fine scale problem is available. In the analysis of the elastoplastic problem, the analytic solution of the fine scale problem is hard to obtain. In this work, we adopted iterative solution procedures by solving the coarse and fine scale problems iteratively. A more detail explanation will be given in Section 4.3.

Remark 1. $\Gamma$is the fine scale switch that notifies nodes that fine scale enrichments are needed. Therefore, it can be considered as a constant and the following property is held:

$$\int_V \Gamma \sum_{\text{all nodes}} (\bullet)\,\mathrm{d}V = \Gamma\int_V \sum_{\text{all nodes}} (\bullet)\,\mathrm{d}V. \tag{69}$$

4.2. Numerical implementations

4.2.1. Moving least-squares approximation

In the meshfree approximation, meshes or elements are not necessary, and only nodes are used for approximation. Meshfree approximation has also reproducing properties. It can reproduce any kind of functions exactly if the bases of the meshfree approximation contain that functions. For these reasons, in the meshfree approximation, adaptivity is easy to implement: *h*-type adaptivity can be implemented by including nodes, and *p*-type adaptivity by increasing the basis function.

The moving least-squares method (Lancaster and Salkauskas, 1981) is the most widely used approximation schemes in meshfree methods. Also, in the present work, the MLS approximation will be employed. In the following, the construction of the MLS shape functions is briefly reviewed with their properties. Let Ω be an open domain of R^d, $d = 1$, 2, or 3. Suppose that a continuous function $u : \overline{\Omega} \to R$ is to be approximated and that its values u_J at the nodal points $x_J \in \overline{\Omega}$, $J = 1, 2, \ldots, N$, are given. A global approximant u^h of u is constructed by first forming, at each point $x \in \overline{\Omega}$, a local approximant $L_x u$, defined in terms of some basis $\{p_i\}_{i=1}^n$, $n \leqslant N$, and a local L^2-norm. It is assumed that the basis satisfies the following properties:

(i) $p_1 = 1$,
(ii) $p_i \in C^r(\Omega)$, $\quad i = 1, 2, \ldots, n$,
(iii) $\{p_i\}_{i=1}^n$ is linearly independent over some set of n of the given N nodal points $x_I \in \overline{\Omega}$.

The linear basis, $p^{\mathrm{T}} = [1, x, y]$, is used throughout the present work.

The local approximant, at each point $x \in \overline{\Omega}$, is defined as

$$L_x u = \sum_{i=1}^{n} a_i(x) p_i. \tag{70}$$

The coefficients $a_i(x)$ are chosen so that $L_x u$ approximates the given function u in a weighted least-squares sense. This yields the following quadratic form:

$$I = \sum_{J=1}^{N} w_J(x)[u(x_J) - (L_x u)(x_J)]^2 = \sum_{J=1}^{N} w_J(x) \left[u_J - \sum_{i=1}^{n} a_i(x) p_i(x_J) \right]^2, \tag{71}$$

where $w_J(x)$, $J = 1, 2, \ldots, N$, are non-negative window functions associated with the nodal point x_J. In the present work, the following quartic spline window function is used:

$$w_J(x) = \begin{cases} 1 - 6r^2 + 8r^3 - 3r^4 & \text{if } r = \|x - x_J\|/h_J \leqslant 1, \\ 0 & \text{if } r = \|x - x_J\|/h_J > 1. \end{cases} \tag{72}$$

where h_J is the influence radius of the nodal point x_J. It can be determined by the product of nodal spacing d and dilatation parameter a_J.

Eq. (71) can be rewritten in the matrix form

$$I = (\mathbf{u} - \mathbf{P}\mathbf{a}(x))^{\mathrm{T}} \mathbf{W}(x) (\mathbf{u} - \mathbf{P}\mathbf{a}(x)), \tag{73}$$

where

$$\mathbf{u}^{\mathrm{T}} = [u_1, u_2, \ldots, u_N], \tag{74}$$

$$\mathbf{P} = \begin{bmatrix} p_1(x_1) & p_2(x_1) & \cdots & p_n(x_1) \\ p_1(x_2) & p_2(x_2) & \cdots & p_1(x_1) \\ \vdots & \vdots & \ddots & \vdots \\ p_1(x_N) & p_2(x_N) & \cdots & p_n(x_N) \end{bmatrix}, \tag{75}$$

$$\mathbf{a}^{\mathrm{T}}(x) = [a_1(x), a_2(x), \ldots, a_n(x)], \tag{76}$$

$$\mathbf{W}(x) = \begin{bmatrix} w_1(x) & 0 & \cdots & 0 \\ 0 & w_2(x) & \cdots & 0 \\ \vdots & \vdots & \ddots & \vdots \\ 0 & 0 & \cdots & w_N(x) \end{bmatrix}. \tag{77}$$

To obtain the coefficients $a(x)$, the quadratic form I is minimized:

$$\frac{\partial I}{\partial \mathbf{a}} = \mathbf{A}(x)\mathbf{a}(x) - \mathbf{B}(x)\mathbf{u} = 0, \tag{78}$$

where

$$\mathbf{A}(x) = \mathbf{P}^{\mathrm{T}} \mathbf{W}(x) \mathbf{P}, \tag{79}$$

$$\mathbf{B}(x) = \mathbf{P}^{\mathrm{T}} \mathbf{W}(x). \tag{80}$$

Thus, the coefficients $a(x)$ are given in the following form:

$$\mathbf{a}(x) = \mathbf{A}(x)^{-1}\mathbf{B}(x)\mathbf{u}. \tag{81}$$

Using the local approximant $L_x u$ of u, the global approximation u^h is defined at each point $x \in \overline{\Omega}$ as follows:

$$u^h(x) = (L_x u)(x) = \sum_{i=1}^{n} a_i(x)p_i(x) = \mathbf{p}(x)^{\mathrm{T}}\mathbf{a}(x), \tag{82}$$

where

$$\mathbf{p}^{\mathrm{T}}(x) = [p_1(x), p_2(x), \ldots, p_n(x)]. \tag{83}$$

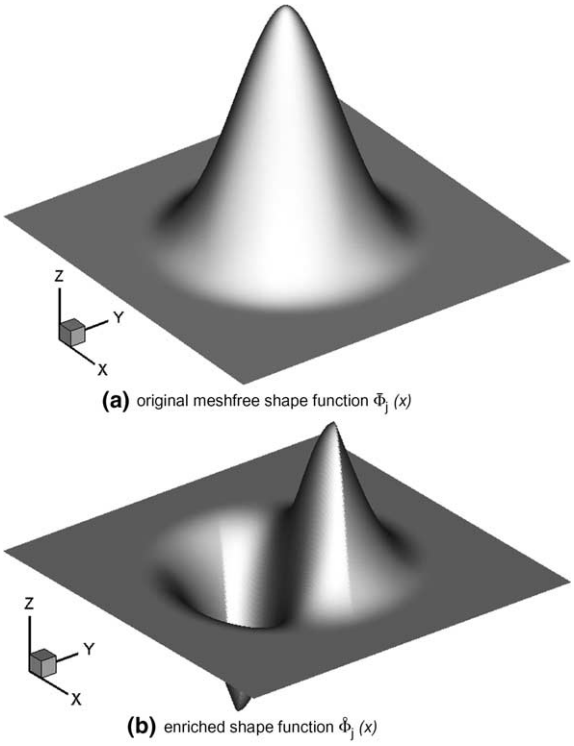

Fig. 2. Shape functions.

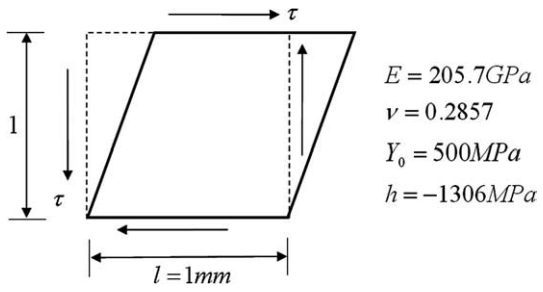

Fig. 3. Pure shear problem.

Using Eq. (81), Eq. (82) can then be expressed as follows:

$$u^h(x) = \sum_{J=1}^{N} \Phi_J(x) u_J, \tag{84}$$

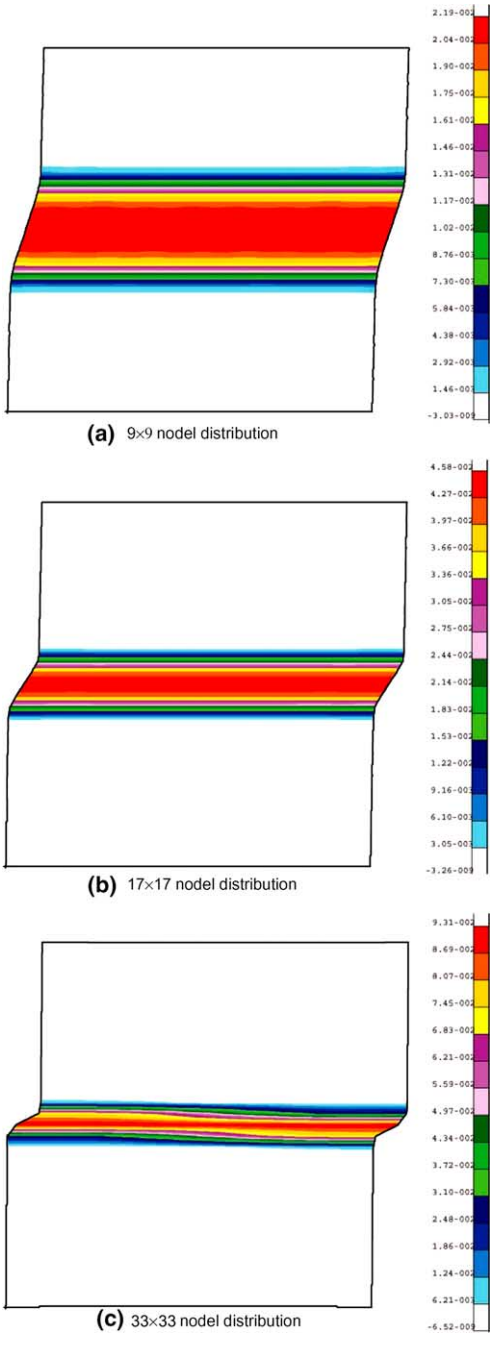

Fig. 4. The distributions of effective plastic strain (meshfree analysis, $a = 1.2$).

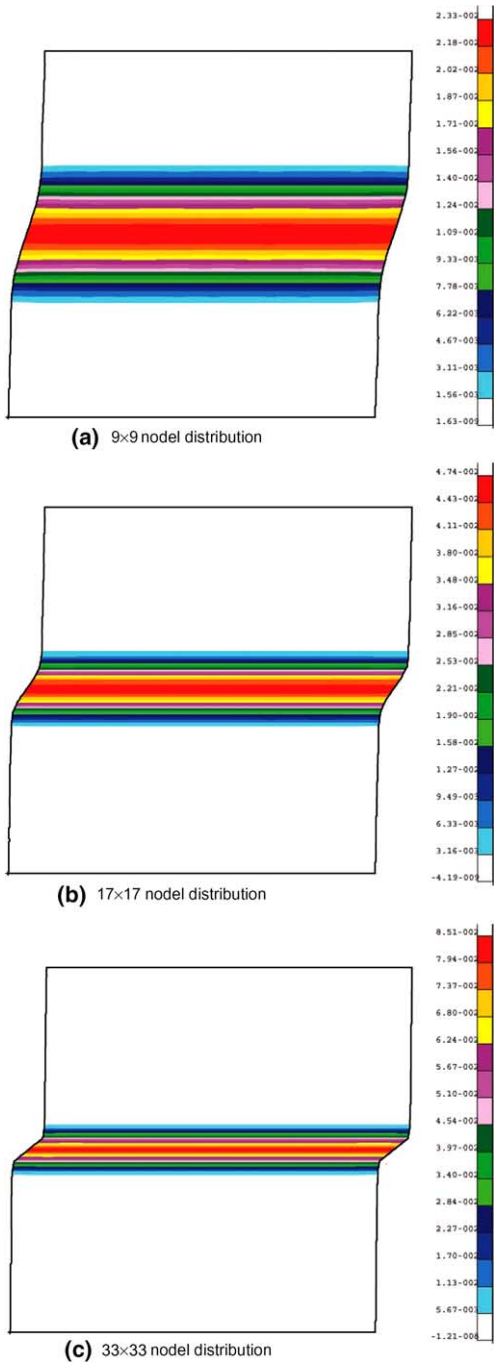

Fig. 5. The distributions of effective plastic strain (meshfree analysis, $a = 2.4$).

where $\Phi_J(x)$ are the MLS meshfree shape functions, which are defined by

$$\Phi_J(x) = \mathbf{p}^{\mathrm{T}}(x)\mathbf{A}^{-1}(x)\mathbf{B}_J(x), \tag{85}$$

where

$$\mathbf{B}_J(x) = w_J(x)\mathbf{p}(x_J). \tag{86}$$

4.2.2. Fine-scale approximation

In this work, as a method of increasing resolution, a partition of unity based extrinsic enrichment is used. Meshfree shape functions have the property of the partition of unity. Let $\Omega \subset R^n$ be an open set and $\{\Omega_i\}$ open cover of Ω. The set of function $\{\varphi_i\}$ defined on $\{\Omega_i\}$ is called the Lipschitz partition of unity if the conditions below are satisfied:

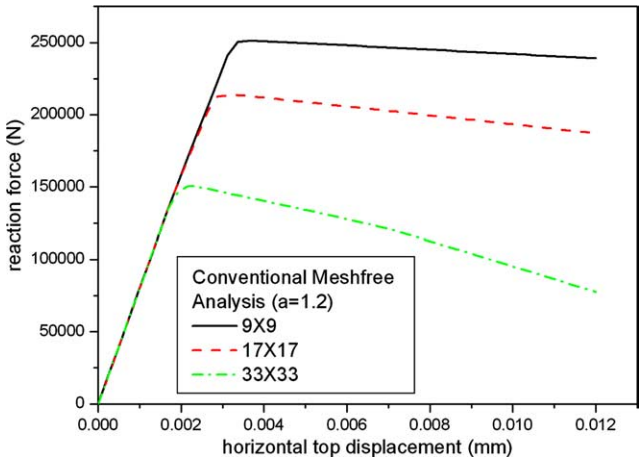

Fig. 6. Load–displacement results of conventional meshfree analysis ($a = 1.2$).

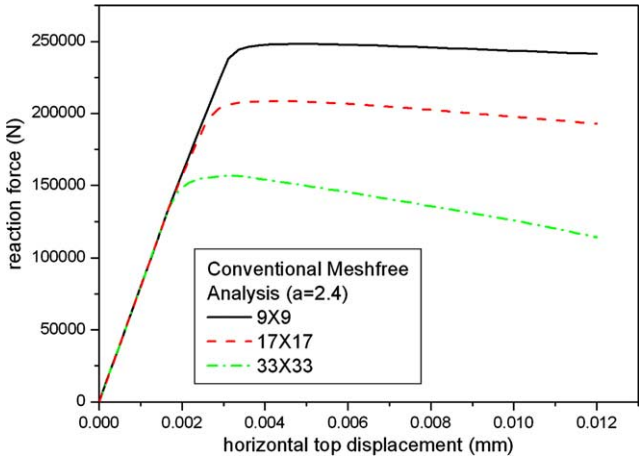

Fig. 7. Load–displacement results of conventional meshfree analysis ($a = 2.4$).

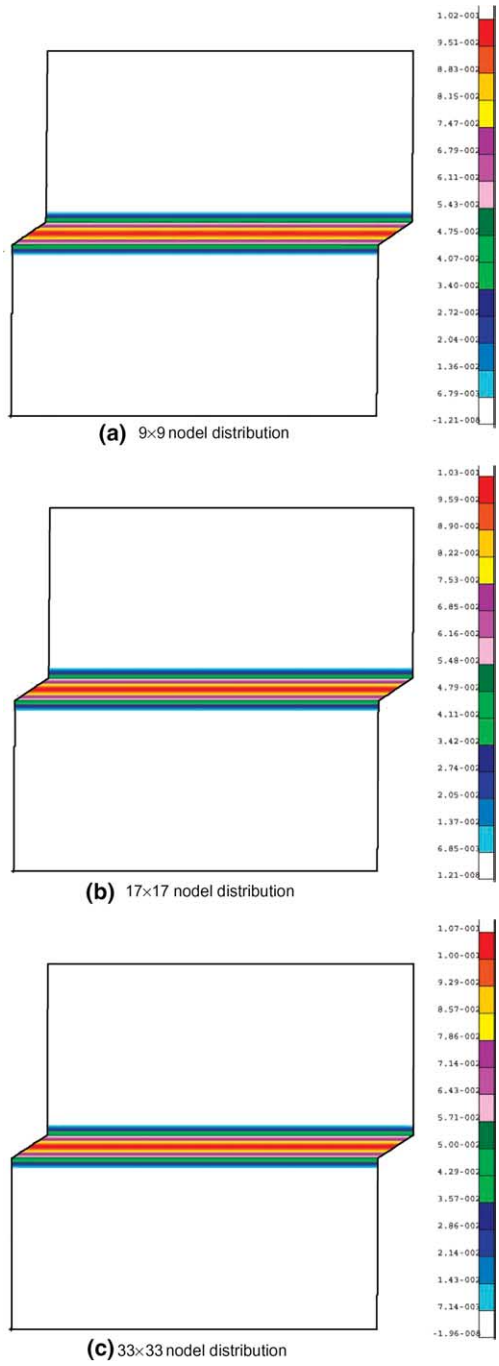

Fig. 8. The distributions of effective plastic strain (multiscale analysis).

(i) $\operatorname{supp}\varphi_i \subset \operatorname{closure}(\Omega_i)$, $\forall i$,
(ii) $\sum_i \varphi_i = 1$ on Ω,

(iii) $\|\varphi_i\|_{L^\infty} \leqslant C_\infty$,
(iv) $\|\nabla\varphi_i\|_{L^\infty} \leqslant C_\infty \frac{C_G}{\mathrm{diam}\Omega_i}$,

where C_∞ and C_G are constants.

Let $V_i \subset H^1(\Omega_i \cap \Omega)$ be given, and then the space

$$V \equiv \sum_i \varphi_i V_i = \left\{ \sum_i \varphi_i v_i \mid v_i \in V_i \right\} \tag{87}$$

is called PUM space. The spaces V_i are referred as the local approximation spaces.

An existing theorem (Babuska and Melenk, 1997) shows that if local approximation spaces have a convergent approximation property of a given function on Ω_i, then PUM space also has a convergent approximation property on Ω.

In the context of above theorem, the approximation form below is available:

$$u^h(x) = \sum_J \Phi_J(x) \left[u_J + \sum_{i=1}^{m} b_{iJ} q_i(x) \right], \tag{88}$$

where $q_i(x)$ are local enriched function and b_{iJ} the coefficients.

As described in Section 3.2, in the localized region, displacement has to be represented as in Eqs. (52) and (53). In these equations, x and y components of displacement are just the scalar multiplication of a function $f_J(x)$ given by

$$f_J(x) = \begin{cases} 1/2 & \text{at } g_J(x) > \delta/2, \\ 1/\delta(-\sin\theta_c(x - x_J) + \cos\theta_c(y - y_J)), & \text{at } |\, g_J(x)\,| \leqslant \delta/2, \\ -1/2 & \text{at } g_J(x) < -\delta/2, \end{cases} \tag{89}$$

where

$$g_J(x) = (-\sin\theta_c(x - x_J) + \cos\theta_c(y - y_J)). \tag{90}$$

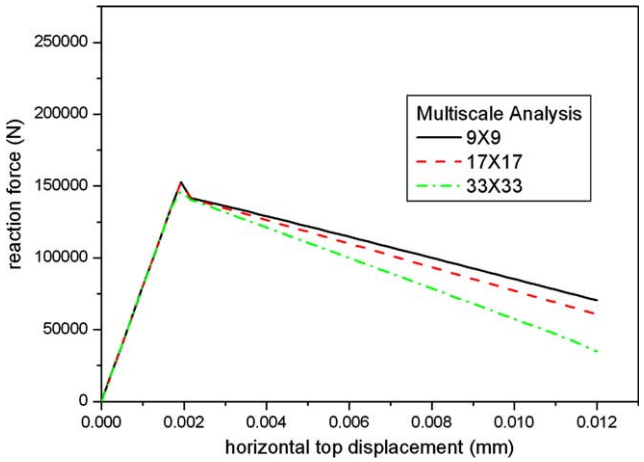

Fig. 9. Load–displacement results of conventional multiscale analysis.

These displacement fields should be embedded to represent the convexification effect. Therefore, as a local enrichment function around node J, $f_J(x)$ is adopted.

Consequently, the following approximation form is possible.

$$u^h(x) = \sum_J \Phi_J(x)\bar{u}_J + \Gamma \sum_J \Phi_J(x) f_J(x)\hat{u}_J = \sum_J \overline{\Phi}_J(x)\bar{u}_J + \Gamma \sum_J \hat{\Phi}_J(x)\hat{u}_J. \tag{91}$$

The first and second term represents coarse and fine scale approximation respectively, and Γ indicates the fine scale switch.

For the two-dimensional case, original meshfree shape function (coarse scale shape function $\overline{\Phi}_J(x)$) and extrinsic enriched shape function for $\theta_c = -30°$ (fine scale shape function $\hat{\Phi}_J(x)$) are plotted in Fig. 2. Enriched shape function have sharp gradient in the localization region with width δ.

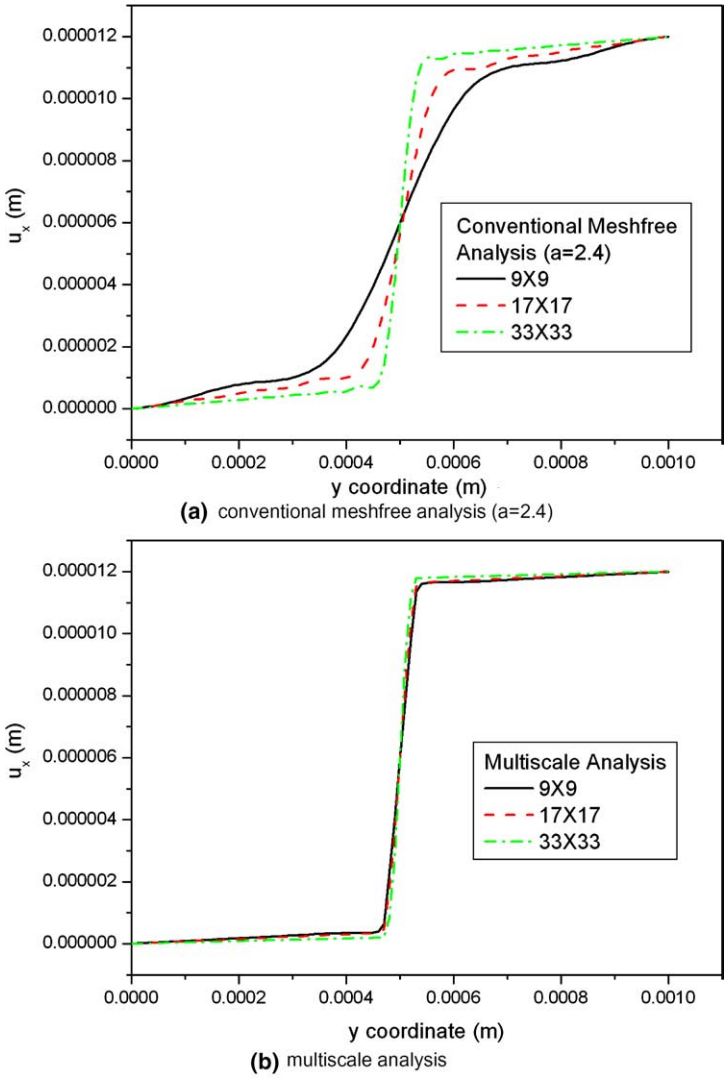

Fig. 10. x-Displacements along the line $x = 0.5$ mm for different nodal distributions.

4.3. Solution procedures

Using the approximation of (91), the coarse scale problem can be written in the matrix form as follows:

$$[K_1^{(n,i)}]\{\Delta\bar{u}^{(n,i+1)}\} = \{F_1^{(n,i)}\} + \{F_2(\Delta\hat{u}^{(n,i+1)})\}, \tag{92}$$

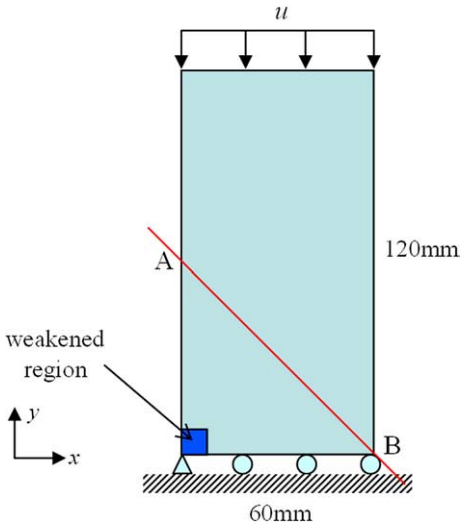

Fig. 11. The compression problem.

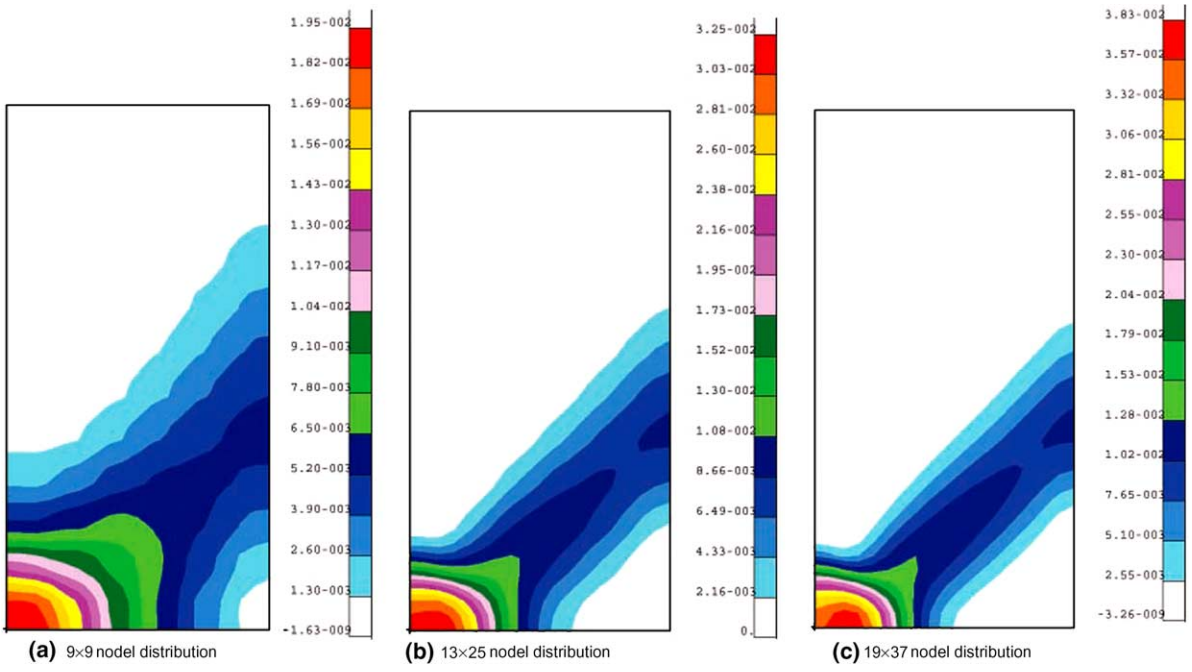

Fig. 12. The distributions of effective plastic strain (meshfree analysis, $a = 1.2$).

where matrix $\lfloor K_1^{(n,i)} \rfloor$ is obtained from left-hand side of Eq. (67), vector $\{F_2(\Delta\hat{u}^{(n,i+1)})\}$ from the right-hand side terms that contain $\Delta\hat{u}^{(n,i+1)}$, and $\{F_1^{(n,i)}\}$ from the rest.

The fine scale problem can also be written in the matrix form as follows:

$$\lfloor K_2^{(n,i)} \rfloor \{\Delta\hat{u}^{(n,i+1)}\} = \{F_3^{(n,i)}\} + \{F_4(\Delta\bar{u}^{(n,i+1)})\}, \tag{93}$$

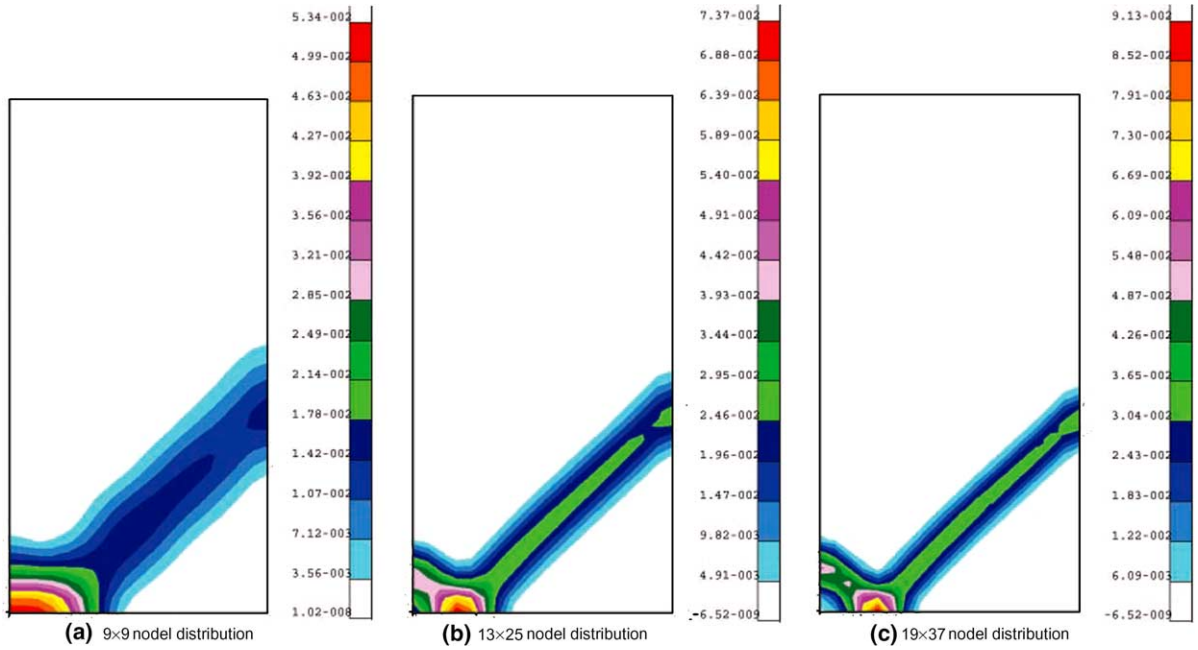

Fig. 13. The distributions of effective plastic strain (meshfree analysis, $a = 2.4$).

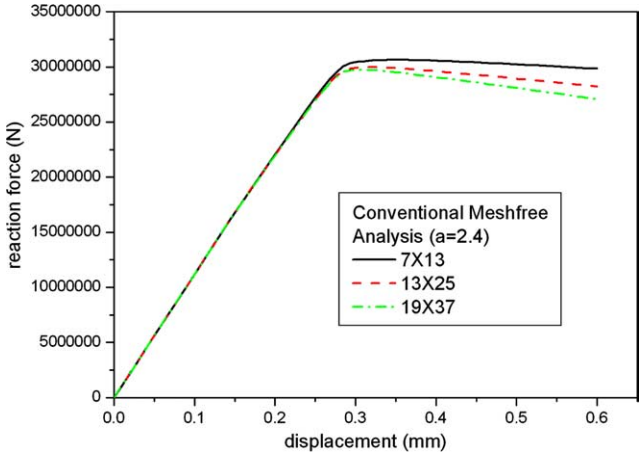

Fig. 14. Load–displacement results of conventional meshfree analysis ($a = 2.4$).

where matrix $\lfloor K_2^{(n,i)} \rfloor$ is obtained from left-hand side of Eq. (68), vector $\{F_4(\Delta\bar{u}^{(n,i+1)})\}$ from the right-hand side terms that contains $\Delta\bar{u}^{(n,i+1)}$, and $\{F_3^{(n,i)}\}$ from the rest. As described in Section 2, the elastoplastic deformation problem described in this work is a non-linear problem, meaning that the problem should be solved iteratively. In this formulation, the coarse scale problem (67) and the fine scale problem (68) are solved iteratively. The solution procedures are summarized as follows.

(1) Solve coarse scale problem by replacing the fine scale variable $\Delta\hat{u}^{(n,i+1)}$ in the right-hand side into $\Delta\hat{u}^{(n,i)}$. Determine $\Delta\bar{u}^{(n,i+1)}$.

$$\lfloor K_1^{(n,i)} \rfloor \{\Delta\bar{u}^{(n,i+1)}\} = \{F_1^{(n,i)}\} + \{F_2(\Delta\hat{u}^{(n,i)})\} \tag{94}$$

(2) Solve the fine scale problem and determine $\Delta\hat{u}^{(n,i+1)}$.

$$\lfloor K_2^{(n,i)} \rfloor \{\Delta\hat{u}^{(n,i+1)}\} = \{F_3^{(n,i)}\} + \{F_4(\Delta\bar{u}^{(n,i+1)})\} \tag{95}$$

(3) Determine total displacement increment and update stress.

$$\Delta u^{(n,i+1)} = \Delta\bar{u}^{(n,i+1)} + \Gamma\Delta\hat{u}^{(n,i+1)} \tag{96}$$

(4) Iterate these procedures until convergence is achieved. (goto (1))
(5) Increase the loading step and find the fine scale region and fine scale approximation function from local failure analysis.
(6) Goto step (1) until the last loading step is reached.

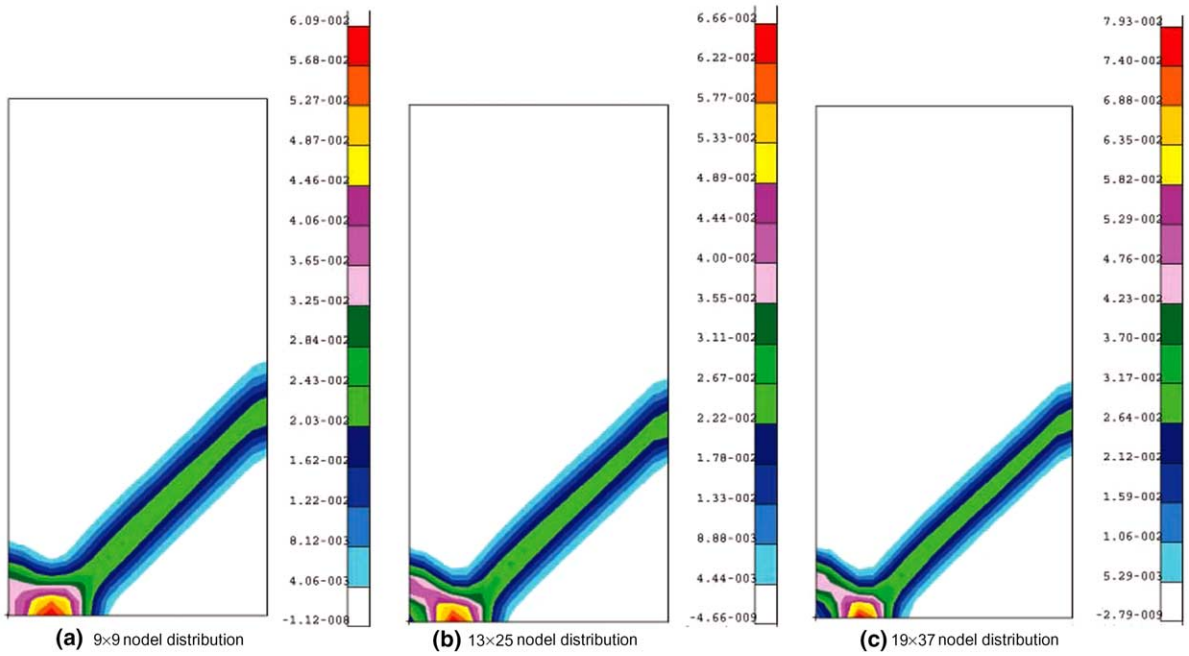

Fig. 15. The distributions of effective plastic strain (multiscale analysis).

5. Numerical examples

In this section, numerical simulations of some problems are presented using the multiscale formulation developed in the previous sections. The constitutive relation of the infinitesimal plastic theory with the J_2 flow rule is adopted. Three benchmark problems are to calculate the developments of the shear bands in a pure shear test, a compression test, and an indentation test under plane strain conditions. For each of them, the results are compared with those of conventional meshfree methods to show the validity of the proposed method.

5.1. Pure shear problem

In the first example, the localization of a specimen subjected to pure shear is investigated. The system is depicted in Fig. 3. A block with a unit length subjected to a shear stress τ is considered. As a plasticity

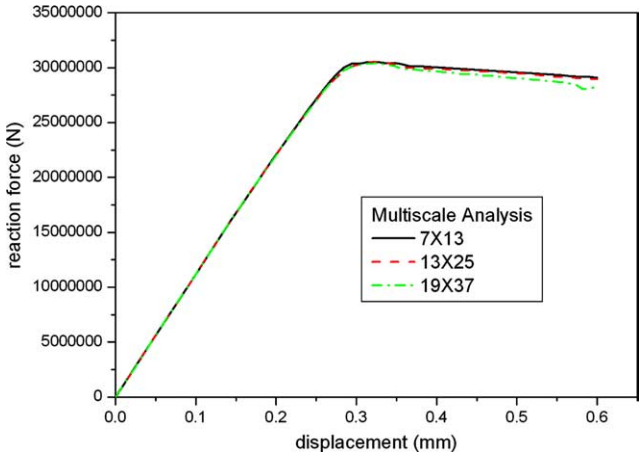

Fig. 16. Load–displacement results of conventional multiscale analysis.

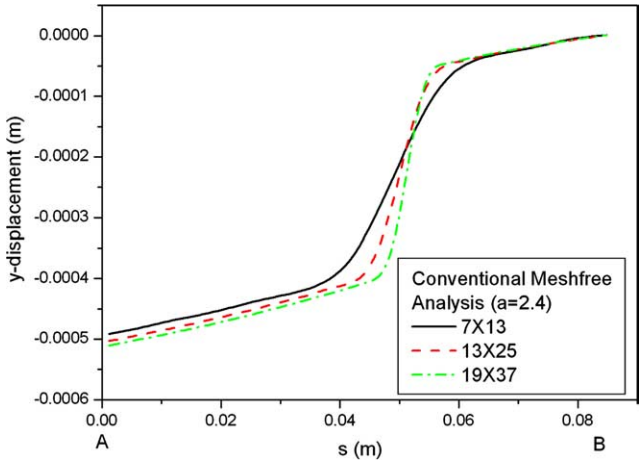

Fig. 17. Meshfree ($a = 2.4$) results of y-displacement along line AB.

model, the J_2 flow rule is used. Young's modulus is set to $E = 205.7$ GPa, Poisson's ration $v = 0.2857$, the initial yield stress $Y_0 = 500$ MPa, and the softening modulus $h = -1306$ MPa. Localization of the homogeneous state is triggered by reducing the yield stress of the middle horizontal row. The given a priori length scale δ is set to 62.5 μm.

The domain is discretized with 9×9, 17×17, and 33×33 uniform nodal distributions. Firstly, this problem is solved using the conventional meshfree method with small and large supports. Dilatation parameters $a = 1.2$ and 2.4 are used for the small and large supports, respectively. The deformed shapes and the distributions of effective plastic strain when the imposed top surface displacement is $u = 0.012$ mm are depicted in Figs. 4 and 5.

As denser nodal distribution is used, displacement changes sharply near the middle horizontal line, and the plastic region is concentrated on the middle horizontal line. In the case of a large support, the effective plastic strain becomes smoother near the middle horizontal line. Figs. 6 and 7 depict the load–displacement curves for different nodal distributions. The results are different obviously for different nodal distributions.

Subsequently, the pure shear problem is solved using the proposed multiscale method. In the construction of multiscale meshfree shape function, small support ($a = 1.2$) is used. The deformed shapes and the distributions of effective plastic strain are almost the same irrespective of nodal distributions (Fig. 8). Load–

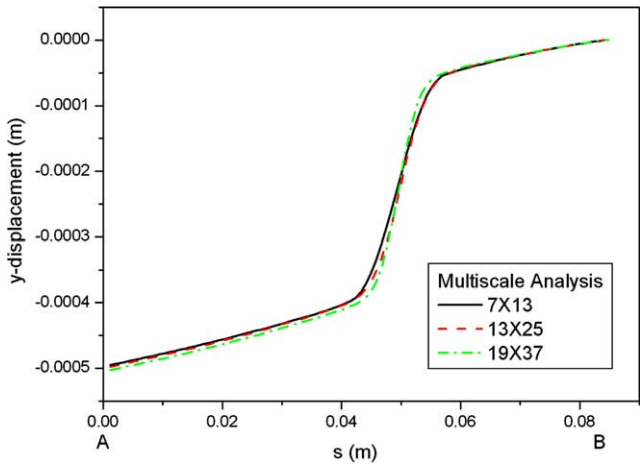

Fig. 18. Multiscale results of y-displacement along line AB.

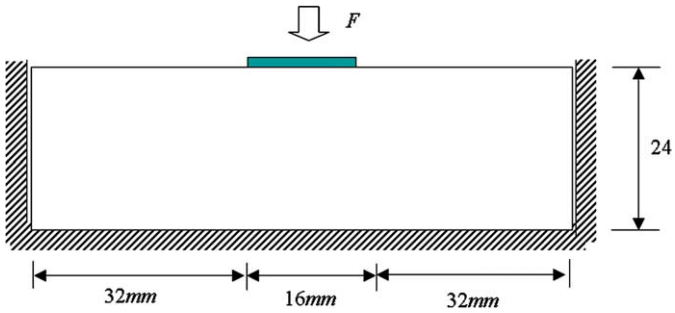

Fig. 19. Indentation test problem.

displacement curves are depicted in Fig. 9. The results are somewhat different, but almost similar, irrespective of nodal distributions.

Fig. 10 depicts x-displacement along the middle vertical line $x = 0.5$ mm. Conventional meshfree results show mesh dependency. However, multiscale results show insensitivity to nodal distributions.

5.2. Compression problem

As a second example, the following compression problem is considered. The geometry and boundary conditions are shown in Fig. 11. The material parameters are the same as in the previous example. The given a priori length scale δ is set to 1.5×10^{-2} m in this example. The weakened region is set on the left bottom corner to initiate softening region by reducing the initial yield stress.

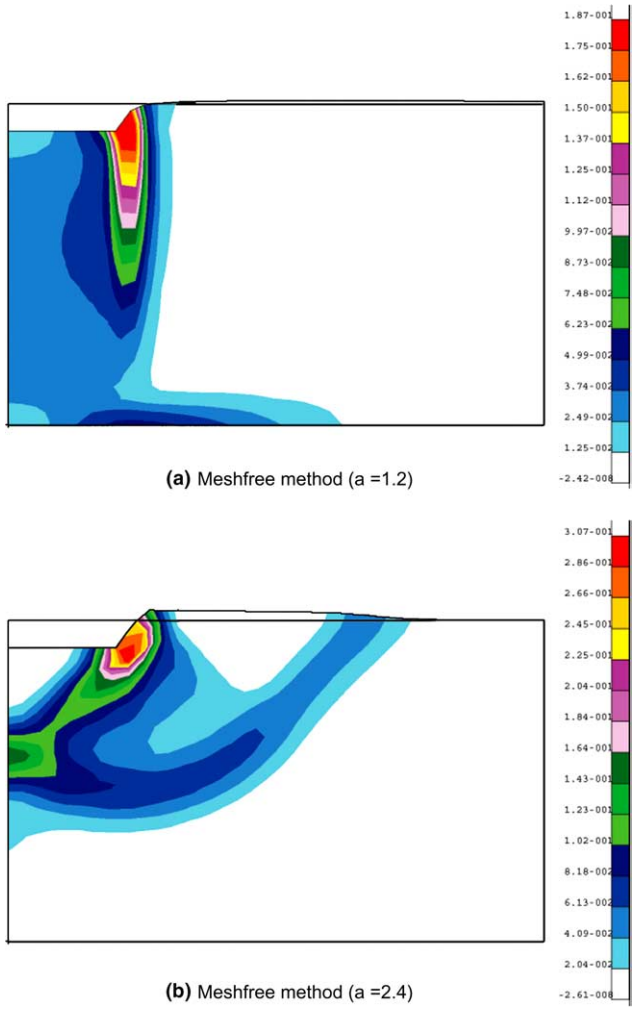

Fig. 20. Distributions of effective plastic strain.

Uniform distribution of 7×13, 13×25, and 19×37 nodes are used. This problem is solved by the proposed multiscale method, and the results are compared with those of conventional meshfree methods of small ($a = 1.2$) and large ($a = 2.4$) supports.

For the case of $u = 0.6$ mm, the resulting distributions of effective plastic strain for the conventional meshfree methods are shown in Figs. 12 and 13. In the case of small support, the plastic regions are spread over the broad area and localized shear bands are not captured. In the case of large support, the plastic region is banded and propagates to a 45° direction from the weakened region. However, the width of the bands varies with nodal distributions. In the denser nodal distributions, thinner bands appear. The load–displacement curves for the meshfree methods with large support are shown in Fig. 14. The results are different for different nodal distributions. In the denser nodal distributions, softer responses are observed.

The resulting distributions of effective plastic strain for the multiscale methods are shown in Fig. 15. The plastic region is banded and the width of shear bands almost invariant. The load–displacement curves are shown in Fig. 16. The results are almost invariant for nodal distributions.

The displacement component along line AB in Fig. 11 is shown in Figs. 17 and 18. In the case of the meshfree method with large support, displacements depend on nodal distribution in some degree. However,

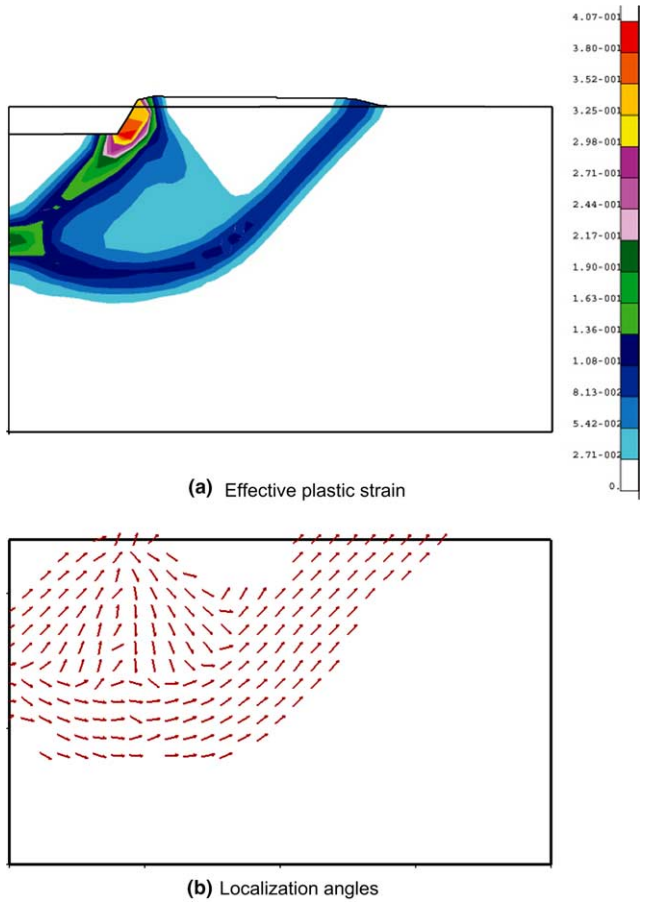

Fig. 21. Distributions of effective plastic strain and localization angles in the case of multiscale method.

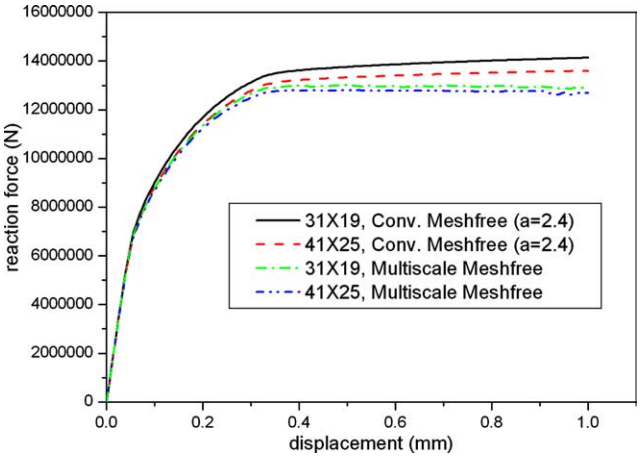

Fig. 22. Load–displacement curves of indentation problem.

in the case of the multiscale method, displacements do not vary much with different nodal distributions, which means that the proposed multiscale method can capture shear band with greater accuracy and yields better results than the meshfree method with large support.

5.3. Indentation problem

The last example is concerned with an analysis of an indentation test under plane strain conditions. The system is depicted in Fig. 19. Displacements on the rigid strip are imposed and reaction forces are calculated. The material properties of the specimen are the same as those of first example except for the softening modulus $h = -131$ MPa. The given a priori length scale δ is set to 2 mm in this example. Due to the symmetry, only one half of the specimen has been analyzed with 30×18 and 40×24 uniform nodal distributions.

For the case of imposed displacement $u = 1$ mm, the resulting distributions of effective plastic strain and deformed shapes are shown in Figs. 20 and 21.

In the case of the conventional meshfree method with small support ($a = 1.2$), unrealistic deformation and plastic strain distributions are observed. In the case of the meshfree method with large support ($a = 2.4$) and the proposed multiscale method, a material pile-up near the rigid strip and curved shear band are observed. Meshfree method with large support has the effect of using high order shape function. Therefore, a regularization effect appears. In the results of the multiscale method, sharp shear bands are observed and the localization angles used in the computation of enrichment functions are in agreement with shear band directions. Fig. 22 shows the load–displacement curves for different nodal distributions. Multiscale results are less stiff and mesh-insensitive than those of the meshfree method with large support.

6. Conclusions

A meshfree multiscale method is presented for efficient analysis of elastoplastic solids. Through the scale decomposition based on variational principles, the problem is decomposed into fine scale and coarse scale problems. The fine scale region is detected from the local failure analysis of an acoustic tensor to indicate region in which deformation changes abruptly. Each scale variable is approximated using a meshfree method associated with a partition of unity. In particular, fine scale approximations are designed to

appropriately represent local behavior using the localization angle. Moreover, regularization effect through convexification of non-convex potential is embedded to represent fine scale behavior. The decomposed problems are solved iteratively. The iteration procedure is indispensable for the analysis of non-linear problems like the elastoplastic deformation problem.

The proposed method is applied to pure shear, compression and indentation problems. Straight and curved shear bands can be effectively captured with the proposed method. The width of the localized region and load–displacement curves are invariant irrespective of nodal distributions, while conventional meshfree results show mesh dependency.

The proposed meshfree multiscale method shows insensitive results to nodal distribution and provides a natural approach to the non-linear problem. This method is useful to the analysis of softening elastoplastic solids. Naturally, use of this method could also be extended to other types of local phenomenon problems not discussed in this paper.

References

Babuska, I., Melenk, J.M., 1997. The partition of unity method. International Journal for Numerical Methods in Engineering 40, 727–758.

Ball, J.M., 1977. Convexity conditions and existence theorems in nonlinear elasticity. Archive of Rational Mechanics and Analysis 63, 337–403.

Bazant, Z.P., 1984. Imbricate continuum and its variational derivation. Journal of Engineering Mechanics, ASCE 110, 1693–1712.

Bazant, Z.P., Lin, F.B., 1988. Non-local yield limit degradation. International Journal for Numerical Methods in Engineering 26, 1805–1823.

Ciarlet, P.G., 1988. Mathematical Elasticity. Elsevier, Amsterdam.

de Borst, R., Sluys, L.J., 1991. Localization in a Cosserat continuum under static and dynamic loading. Computer Methods in Applied Mechanics and Engineering 90, 805–827.

Garikipati, K., Hughes, T.J.R., 1998. A study of strain localization in a multiple scale framework–The one-dimensional problem. Computer Methods in Applied Mechanics and Engineering 159, 193–222.

Garikipati, K., Hughes, T.J.R., 2000. A variational multiscale approach to strain—formulation for multidimensional problems. Computer Methods in Applied Mechanics and Engineering 188, 39–60.

Hadamard, J., 1903. Lecons sur la propagation des ondes et les equations de l'hydrodynamique. Hermann, Paris.

Hughes, T.J.R., 1995. Multiscale phenomena: Green's function, the Dirichlet-to-Neumann formulation, subgrid scale models, bubbles and the origins of stabilized methods. Computer Methods in Applied Mechanics and Engineering 127, 387–401.

Hughes, T.J.R., Feijoo, G.R., Mazzei, L., Quincy, J.-B., 1998. The variational multiscale method—a paradigm for computational mechanics. Computer Methods in Applied Mechanics and Engineering 166, 3–24.

Hughes, T.J.R., Oberai, A.A., Mazzei, L., 2001a. The multiscale formulation of large eddy simulation: Decay of homogeneous isotropic turbulence. Physics of Fluids 13, 505–512.

Hughes, T.J.R., Oberai, A.A., Mazzei, L., 2001b. Large eddy simulation of turbulent channel flows by the variational multiscale method. Physics of Fluids 13, 1784–1799.

Lancaster, P., Salkauskas, K., 1981. Surface generated by moving least-squares methods. Mathematics of Computation 37, 141–158.

Li, S., Liu, W.K., 1999a. Reproducing kernel hierarchical partition of unity. Part I: Formulation and theory. International Journal for Numerical Methods in Engineering 45, 251–288.

Li, S., Liu, W.K., 1999b. Reproducing kernel hierarchical partition of unity. Part II: Application. International Journal for Numerical Methods in Engineering 45, 289–317.

Liu, W.K., Chen, Y., 1995. Wavelet and multiple scale reproducing kernel methods. International Journal for Numerical Methods in Engineering 21, 901–931.

Liu, W.K., Chen, Y., Uras, R.A., Chang, C.T., 1996. Generalized multiple scale reproducing kernel particle methods. Computer Methods in Applied Mechanics and Engineering 139, 91–157.

Miehe, C., 2000. Strain-driven homogenization of inelastic microstructures and composites based on an incremental variational formulation. International Journal for Numerical Methods in Engineering 55, 1285–1322.

Miehe, C., Lambrecht, M., 2003. A two-scale finite element relaxation analysis of shear bands in non-convex inelastic solids: small-strain theory for standard dissipative materials. Computer Methods in Applied Mechanics and Engineering 192, 473–508.

Morrey, C.B., 1952. Quasi-convexity and the semicontinuity of multiple integrands. Pacific Journal of Mathematics 2, 25–53.

Muhlhaus, H.B., Aifantis, E.C., 1991. A variational principle for gradient plasticity. International Journal of Solids and Structures 28, 845–858.

Muhlhaus, H.B., Vardoulaks, I., 1987. The thickness of shear bands in granular materials. Geotechnique 37, 271–283.
Needleman, A., 1988. Material rate dependence and mesh sensitivity in localization problems. Computer Methods in Applied Mechanics and Engineering 67, 69–85.
Oberai, A.A., Pinsky, P.M., 1998. A multiscale finite element method for the Helmhotz equation. Computer Methods in Applied Mechanics and Engineering 154, 281–297.
Oden, J.T., Vemaganti, K., Moes, N., 1999. Hierarchical modeling of heterogeneous solids. Computer Methods in Applied Mechanics and Engineering 172, 3–25.
Oden, J.T., Zohdi, T.I., 1997. Analysis and adaptive modeling of highly heterogeneous elastic structures. Computer Methods in Applied Mechanics and Engineering 148, 367–391.
Ortiz, M., Leroy, Y., Needleman, A., 1987. A finite element method for localized failure analysis. Computer Methods in Applied Mechanics and Engineering 61, 189–214.
Simo, J.C., Hughes, T.J.R., 1998. Computational Inelasticity. Springer-Verlag, New York.
Zbib, H.M., Aifantis, E.C., 1988. On the localization and postlocalization behavior of plastic deformation. Res Mechanica 23, 261–305.
Zienkiewicz, O.C., Taylor, R.L., 1989. Finite Element Method, Fourth ed. McGraw Hill, London.
Zohdi, T.I., Oden, J.T., Rodin, G.J., 1996. Hierarchical modeling of heterogeneous bodies. Computer Methods in Applied Mechanics and Engineering 138, 273–298.